J Appl Electrochem (2012) 42:21–29
DOI 10.1007/s10800-011-0367-z

ORIGINAL PAPER

Cathodic degradation mechanisms of pure Sn electrocatalyst in a nitrogen atmosphere

L. M. Chiacchiarelli · Y. Zhai · G. S. Frankel · A. S. Agarwal · N. Sridhar

Received: 29 August 2011 / Accepted: 29 October 2011 / Published online: 26 November 2011

Abstract The application of electrocatalysts used at high cathodic overpotentials for the electrochemical reduction of pollutant species such as CO_2 has revealed a lack of understanding of the cathodic degradation mechanisms of those materials. Pure Sn is one of the most relevant candidate materials mainly because of its high selectivity for the reduction of CO_2 to formic acid and formate salts. Degradation of the electrocatalyst can arise from a combination of cathodic polarization and induced changes to the surface by CO_2 reduction products. In this study, the cathodic degradation mechanisms of pure Sn were studied as a function of rotation rate, time, current density, electrolyte concentration, grain size, and orientation in a nitrogen-saturated atmosphere using a rotating disk electrode. Several degradation morphologies were observed, but three were dominant. In the first type, electrochemical alterations of grains with specific orientations produced substantial weight changes, both losses and gains. The second type resulted in an alkali-rich deposit that had a high coverage but produced small weight changes. The third type consisted of carbon-rich stains that typically had a small coverage.

Keywords Sn degradation · Cathodic corrosion · Sn corrosion · Electrocatalyst · Deposit formation · Electrochemical reduction

L. M. Chiacchiarelli · G. S. Frankel (✉)
Fontana Corrosion Center, The Ohio State University, Columbus, OH 43210, USA
e-mail: frankel.10@osu.edu

Y. Zhai · A. S. Agarwal · N. Sridhar
DNV Research and Innovation, Dublin, OH 43017, USA

1 Introduction

Technologies involving the electrochemical recycling of pollutants have recently seen renewed emphasis. Examples include the reduction of nitrate in nuclear waste or drinking water to nitrogen gas [1–4] and the electrochemical reduction of CO_2 to useful products, such as formate [5–7]. To drive the reaction at a substantial rate and selectivity, these technologies typically involve the application of high cathodic overpotentials (~ -2 V vs. NHE). Furthermore, to obtain high selectivity in aqueous electrolytes, electrocatalysts with a low exchange current density for hydrogen evolution have been the main candidates, e.g., Sn, Pb, In, Sb. However, the application of cathodic potentials also results in reactions that cause degradation of the electrocatalysts [2]. This degradation can limit electrocatalyst lifetime and thus adversely affect the economics of those technologies. The cathodic degradation behavior of metals in general has not been studied extensively. Most of the literature related to cathodic degradation mechanisms was published before the 1980s [8–11]. The decrease of electrocatalyst performance can arise from several sources: (i) cathodic degradation of the catalyst surface [8–11, 17–25], (ii) deposition of non-catalytic species from the reaction intermediates of the reduction of the pollutant species [12–16], (iii) deposition of non-catalytic metallic species from contaminants in the electrolyte [12], and (iv) anodic degradation of catalyst at sites where gas bubbles form preventing the cathodic polarization of the catalyst; In this article, the cathodic degradation of electrocatalyst metal is considered.

Cathodic degradation of the electrocatalyst surface has been considered to be limited to metals with a high overpotential for H_2 evolution (Sn, Pb, Sb, etc.) [8]. The cathodic corrosion of Sn electrodes was studied by

Salzberg and Mies [10] who found that weight loss was proportional to the amount of charge passed through the electrode, confirming Faradaic behavior. The rate of cathodic corrosion was significant for current density levels on the order of A cm^{-2} and was time independent. The disintegration rate was dependent on the cationic species present. For example, small additions of RuCl or CsCl substantially decreased the rate. Most of the lost Sn from the electrode was found as colloidal Sn in the solution instead of a gaseous Sn hydride. Finally, the lack of good reproducibility was emphasized, even though precautions were taken regarding deaeration and purity of electrolyte and electrode. Salzberg [10] hypothesized the formation of an unstable SnH_2 intermediate that can either be decomposed into colloidal Sn or into SnH_4(g). The intermediate formula was calculated from the weight loss rate.

Katsounaros et al. [2] trapped SnH_4(g) in a silver nitrate solution and measured the Sn content with Atomic Absorption Spectroscopy. Measurable concentrations of SnH_4(g) were only found for potentials more negative than −2.4 V versus Ag/AgCl. The surface roughness increased and reached a steady state after several cathodic polarization experiments. The extent of cathodic corrosion was found to depend strongly on the ionic species in solution, with a substantial decrease of cathodic disintegration observed with the addition of nitrate or ammonium ions.

Gladyshev [8] developed a unifying theoretical approach toward the cathodic disintegration of metals by proposing an intermediate of the reaction, metallide anion M^{n-}. The key aspect of this mechanism is that it covers the possibility of forming either colloidal M, M hydrides or spongy deposits depending on the chemical interaction of those metallide anions. However, no spectroscopic study has identified this proposed intermediate.

Degradation of electrocatalysts by electrochemical incorporation is based on the insertion of cationic species present in the electrolyte (mainly alkalis) into the electrode surface. This is a well-known phenomenon in batteries, where the incorporation is reversible and is useful as a charge transfer mechanism [12]. The incorporation is easily identifiable in voltammograms in non-aqueous solvents because of the lack of competing reactions. However, in aqueous solutions, high cathodic potentials can trigger other possible reactions (hydride formation, hydrogen evolution, etc.), which complicate the analysis of the voltammogram. In addition, the deposits formed are usually unstable in aqueous solutions. Kiseleva et al. [13] studied the cathodic incorporation of Li^+ and Na^+ into Sn electrodes. After the application of a cathodic potential, the subsequent anodic step resulted in a plateau at a specific potential, indicating that an intermetallic formed during the cathodic step was being decomposed. Several other studies regarding the formation of intermetallics on Sn can be found in the literature [14–16]. Courtney used an in situ X-ray technique to prove the formation of intermetallics [17].

From a thermodynamic point of view, alkali hydrides ($KH_{(s)}$, $NaH_{(s)}$, $LiH_{(s)}$) can form at potentials more negative than about −1.4 V versus NHE in neutral aqueous electrolytes [18]. These alkali hydrides are generally very unstable compounds [19] that, in the presence of water or oxygen, react exothermically to form hydrogen. Therefore, the formation of alkali hydrides would result in lower selectivity but not cause degradation. However, recent results have proven the formation of stable alkali hydrides, which might decrease the active electrode area [20].

Because the electrode is polarized at high cathodic potential, hydrogen evolution is an inevitable phenomenon and gas bubbles will evolve from the surface. The bubble population on the surface of the electrode decreases the effective area of the electrode and might accelerate degradation mechanisms by an effective increase in current density [21, 22]. Using the definition of bubble coverage, Θ, given by Eigeldinger [21], the current density, *I*/*A*, will be modified to a value of *j* according to:

$$j \equiv \frac{I}{A}\frac{1}{1-\Theta} \tag{1}$$

A large bubble coverage can therefore result in a substantial increase in current density. For example, coverage of 30% causes a 40% increase in current density.

Cathodic degradation of pure Sn was investigated in this study using solutions saturated with N_2; work on solutions containing CO_2 will be presented separately. This study will focus on reactions that cause degradation by the formation of either a deposit or by corrosion. It will be shown that the cathodic degradation of Sn is a complex process. The different types of attack are classified in an attempt to clarify the various phenomena and bring focus on the important degradation modes.

2 Experimental

All experiments were carried out using a PAR analytical cell (RDE0018) in which an inverted cup water seal (Fig. 1) was implemented to reduce oxygen contamination. The electrolyte volume was 50 mL. The sample was a rotating disk electrode (RDE). The rotator system was a PAR 636 with rotation rates going up to 3,000 rpm. A Pine Instruments AFE3M shaft and an acrylic standard ChangeDisk RDE tip were used. The ferricyanide/ferrocyanide reversible couple was used to test the RDE system.

The electrochemical experiments were performed using a CH710 potentiostat (CH Instruments). A three-electrode configuration was used, where the reference electrode was

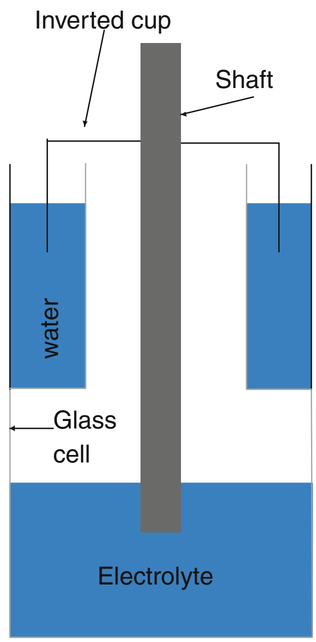

Fig. 1 Schematic of inverted cup water seal implemented in the experiments. A rotating acrylic cylinder was attached to the shaft and submerged in a water compartment

an Accumet Saturated Calomel Electrode and the counter electrode was a Pt wire separated from the working electrode by a Nafion membrane (Ion Power N117). The working electrode consisted of a 4.9 mm diameter Sn (99.9985%, Puratronic) disk embedded in an acrylic tip. The samples were polished to 0.05 µm using a Struers Rotopol-15 automatic polishing machine, then rinsed and cleaned in a DI water ultrasonic bath. A control sample was set aside for each 10 samples prepared to check that the surface was free of abrasive particles embedded in the matrix. In addition, an optical micrograph of each sample was taken before each experiment. The pH measurement was performed in situ using an Oakton Accorn series pH meter coupled with an Accumet pH electrode.

Grain size was controlled by changing the polishing procedure and by heat treatment. To obtain a small grain size distribution (~50 µm), the polishing time at high grit sizes was longer than to obtain a medium grain size distribution (~700 µm). For large grain sizes (~1 mm), a heat treatment at 170 °C for 1 h was performed. It is important to notice that grain size distribution was uniform only at low and high grain sizes.

The cell was deaerated for at least 30 min before each experiment with N_2 (99.998%) gas that was first passed through moisture (ColeParmer), hydrocarbon (Restek), and oxygen (Restek) traps. The gas tubing was made of stainless steel. The weight measurements were performed using a Sartorius BP210D scale which was calibrated using an externally calibrated weight. Optical characterization was performed using a Quanta 200 SEM. The orientation of crystalline grains was obtained using a TSL Electron Backscatter Diffraction (EBSD) system. X-ray photoelectron spectroscopy (XPS) was performed with a Kratos Axis Ultra XPS. All solutions were made with reagent grade chemicals and deionized water (18.2 MΩ cm) from a Millipore system.

Galvanostatic experiments at two cathodic current densities were performed, high (175 mA cm^{-2}) and moderate (87.5 mA cm^{-2}), and the effects of rotation rate, time, grain size and orientation, and electrolyte concentration on degradation morphology and extent were studied. Due to the high cathodic current densities, a population of bubbles forming and detaching at the edges of the Sn disk was observed, especially in low rotation rate experiments (500 rpm). To avoid excessive accumulation of bubbles, the holder was machined in acrylic which is less hydrophobic than Teflon. A Luggin probe was used to measure the potential at a distance of about 15 mm from the electrode surface. However, the combination of a high bubble coverage and a high current density complicated the measurement of the real surface potential.

3 Results

The experiments showed several types of degradation morphology, which were classified according to their appearance in the SEM and elemental composition obtained from energy dispersive X-ray spectroscopy (EDS). The morphologies are labeled G (grain etching/corrosion), D (deposit formation), and B (black deposits). The G type morphology can be observed in Fig. 2a. The surface reflected the grain structure of the Sn electrode with evidence of etching, the extent of which varied from grain to grain. As will be shown, the weight change of this type of morphology also varied considerably, with both weight gain and loss observed in repeated experiments under the same conditions. This degradation morphology was not dependent on grain size, but strongly on grain orientation.

The D type morphology was associated with a deposit as shown in Fig. 2b, c. This degradation product was usually accompanied by small weight changes. The coverage was usually high and not dependent on grain size and orientation. Two different D type morphologies were identified. D1 deposits (Fig. 2b) were larger, usually in the 10–100 µm range, whereas D2 deposits (Fig. 2c) were usually less than 20 µm in size. Despite the dimensions, both were able to cover a substantial portion of the electrode area. In addition, this deposit was found both directly on the unaltered Sn surface and on top of a G type degraded surface.

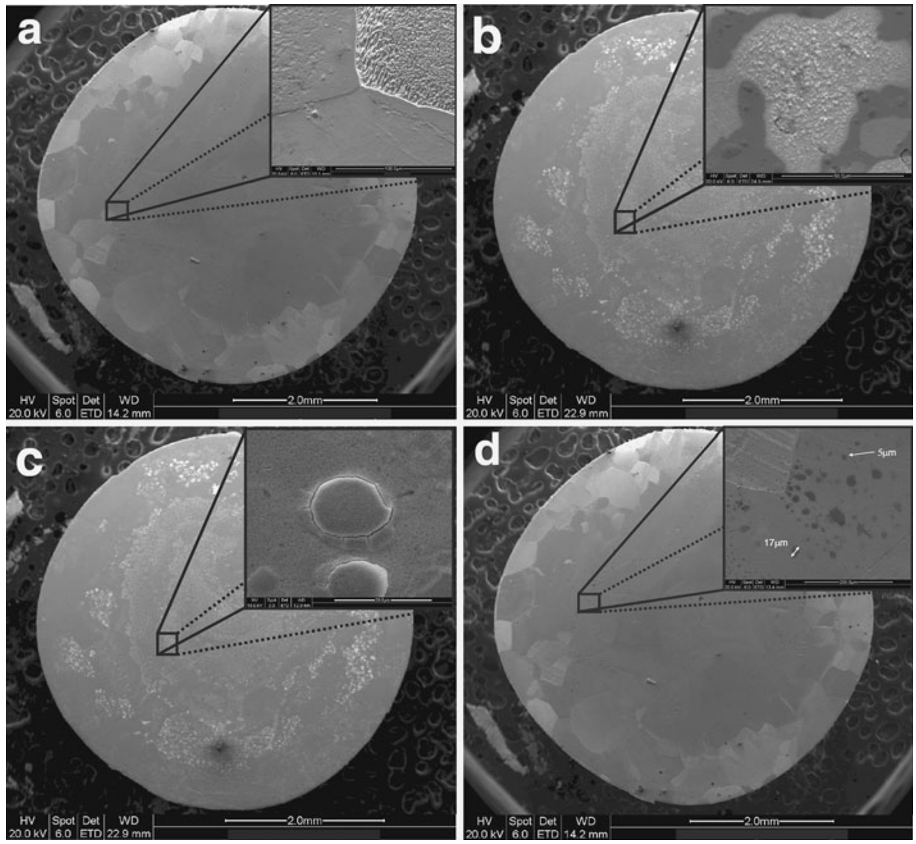

Fig. 2 SEM images of the different types of degradation: **a** G, **b** D1, **c** D2, and **d** B. Samples polarized galvanostatically at 175 mA cm^{-2}. The time was 10 min for (**a**) and 60 min for the other cases. The solution was 0.5 M $KHCO_3$. The grain size was small for (**a**) and medium for the other cases. The rotation rate was 500 rpm for (**a**, **d**) and 3,000 rpm for (**b**, **c**)

The B type is shown in Fig. 2d. This deposit appeared to be a stain on the surface of the electrode. The coverage was usually not high but the B type deposit could be present with either G or D type surfaces. The size was usually small, on the order of 1–10 μm.

3.1 Parametric influences

Nine experiments were performed to evaluate the effect of rotation rate on weight loss rate (WLR) and degradation morphology. The electrolyte was 0.5 M $KHCO_3$ and the electrode had a medium grain size. The experiments were performed at a high current density (175 mA cm^{-2}) for 60 min. The WLR as a function of rotation rate is shown in Fig. 3a. At low and high rotation rates, there was a large dispersion in WLR. However, the WLR tended to increase with increasing rotation rate. Weight gain was measured for the samples at the slowest rate of 500 rpm, whereas the WLR ranged from 10 to 20 mg cm^{-2} h^{-1} at 3,000 rpm. The degradation morphology was also strongly dependent on rotation rate. At 500 rpm the morphology was primarily of the G type (Fig. 3b), while a mixed G, D type was observed at 1,500 rpm (Fig. 3c). At 3,000 rpm, a very fine structure of D and B type with a high coverage was observed (Fig. 3d). Underneath this fine structure, G type was found (etched grains which exhibit different contrast in Fig. 3d). The measured potential reached a diffusion controlled steady-state value of −3 to −3.2 V versus SCE (Fig. 3e). The potential started at less negative values and the transition time to the steady state generally decreased with increasing rotation rate. At slower rotation rate, the potential started at less negative values and a transition period was observed before the steady-state value was attained. The transition time to the steady state generally decreased with increasing rotation rate, which is associated with a change from G to D type as a function of increasing rotation rate (as previously observed). At the nominal steady state, the potential continued to drift in the positive direction at about 1 mV min^{-1}.

A series of experiments was performed to analyze the effect of time on WLR and degradation morphology. A 0.5 M $KHCO_3$ solution was used with a small grain size electrode. The experiments were performed at the high current density (175 mA cm^{-2}) for 5, 10, or 30 min at 500 or 3,000 rpm. The WLR as a function of time and rotation rate is shown in Fig. 4a. At a given time, the WLR increased with increasing rotation rate, as was also shown in Fig. 3. In addition, the WLR decreased with time, and the rate of decrease slowed with time. Figure 4b–d shows the sample surfaces. At short times, the degradation morphology was mainly of the G type, while at higher times D type was also observed. The G or D type deposits covered

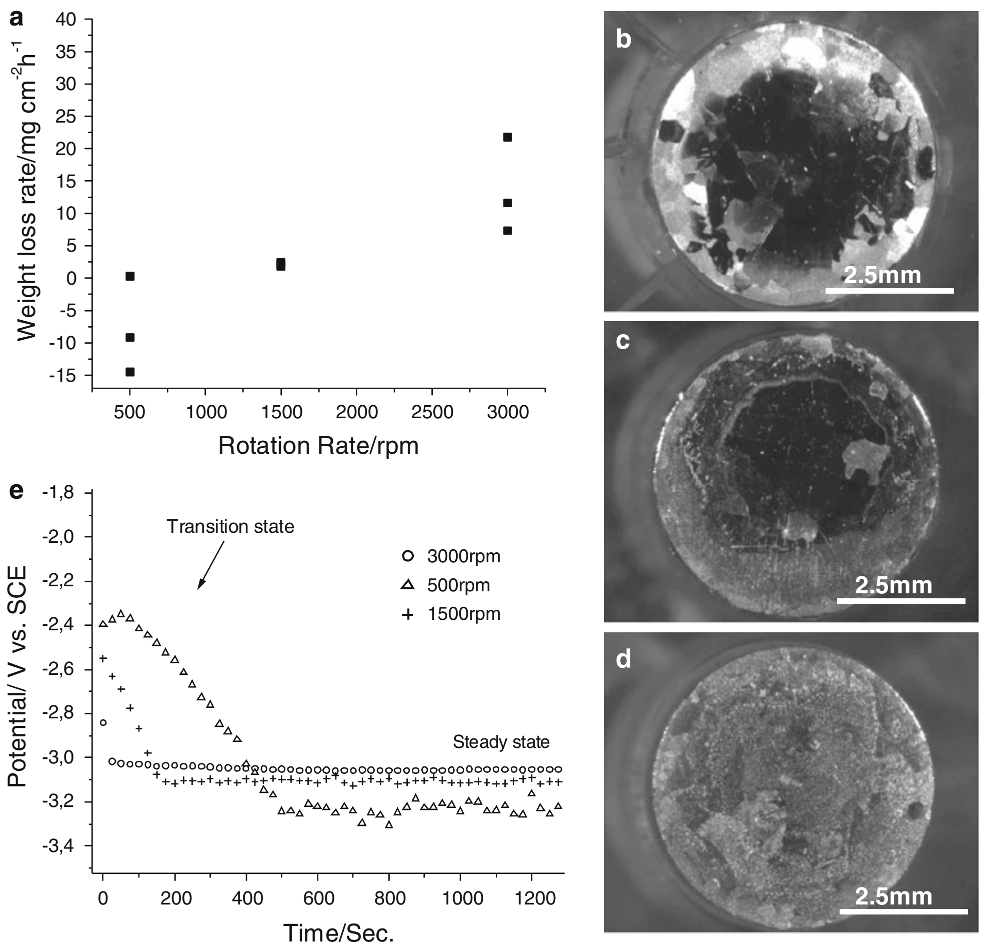

Fig. 3 Results of galvanostatic experiments at 175 mA cm^{-2}, 0.5 M $KHCO_3$, medium grain size, and 60 min. **a** weight loss rate (negative is weight gain) as a function of rotation rate, **b** surface of sample tested at 500 rpm, **c** surface of sample tested at 1,500 rpm, **d** surface of sample tested at 3000 rpm, **e** potential as a function of time (only one curve for each rotation rate is shown to avoid confusion)

the whole surface of the electrode. Though not shown, the potential showed the same tendencies with time as described above, such as transition times, an increase in the nominal steady-state potential with increasing rotation rate, and a slight anodic trend at steady state.

To study the effect of grain size on degradation morphology, grain growth was induced by heat treatment at 170 °C for 1 h in an air atmosphere. Grain growth was substantial, from around 10 μm to the range of mm. Even though the sample was not a single crystal with one orientation, the number of grain orientations on the electrode surface was greatly reduced. A set of identical galvanostatic experiments at the high current density (175 mA cm^{-2}) in 0.5 M $KHCO_3$ for 10 min was performed and the results showed a large dispersion in WLR, from −29.1 to +121.8 mg cm^{-2} h^{-1}. The degradation morphology (Fig. 5b–d) was predominantly of the G type when a high positive WLR was measured and a combination of D and B type when a negative WLR was measured. This indicates that grain orientation controls the type and extent of degradation, particularly for the G type. The open circuit potential (OCP) transient measured immediately after the cathodic polarization for samples with a positive WLR exhibited a shoulder at approximately −1.1 V SCE (Fig. 5a), indicating possible formation of a metastable intermediate on the surface that decomposed within minutes.

To examine the orientation dependence of the G type, the electrode surface was analyzed with EBSD. As shown in Fig. 6, orientations between [001] and [110] were susceptible to G type corrosion.

Experiments performed in dilute bicarbonate solution (10 mM) exhibited a decrease in the magnitude of WLR independent of rotation rate, Fig. 7. In other words, the WLR was close to zero at 500 and 3,000 rpm in this solution, while the polarity of the WLR was different for the two rotation rates in the 0.5 M solution. In addition, the morphology in the dilute solution was of the G type and it was found only on the edges of the disk. The pH increased from 9.5 to about 11.0 after the experiment. Furthermore, the increase in pH was higher for lower rotation rates. In contrast, the pH change for experiments in 0.5 M $KHCO_3$ was less than 0.3 units.

Decreasing the current density from the high (175 mA cm^{-2}) to the medium (87.5 mA cm^{-2}) resulted in a decrease in the magnitude of WLR independent of

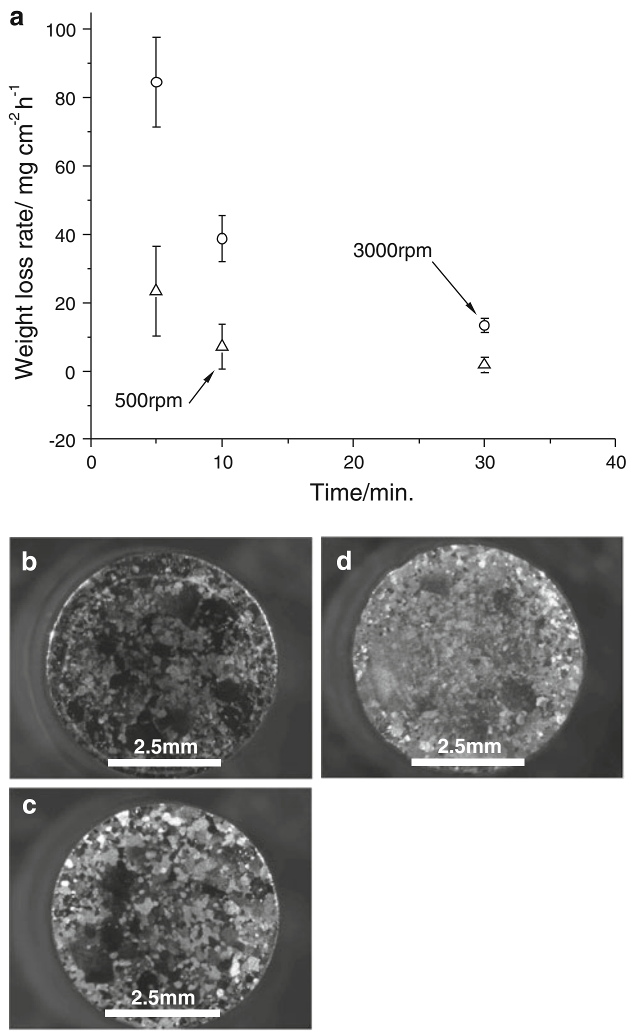

Fig. 4 Results of galvanostatic experiments at 175 mA cm^{-2} in 0.5 M $KHCO_3$ for small grain size sample: **a** Weight loss rate as a function of time and rotation rate; surface of sample tested at 500 rpm for 5 min (**b**), 10 min (**c**), and 30 min (**d**)

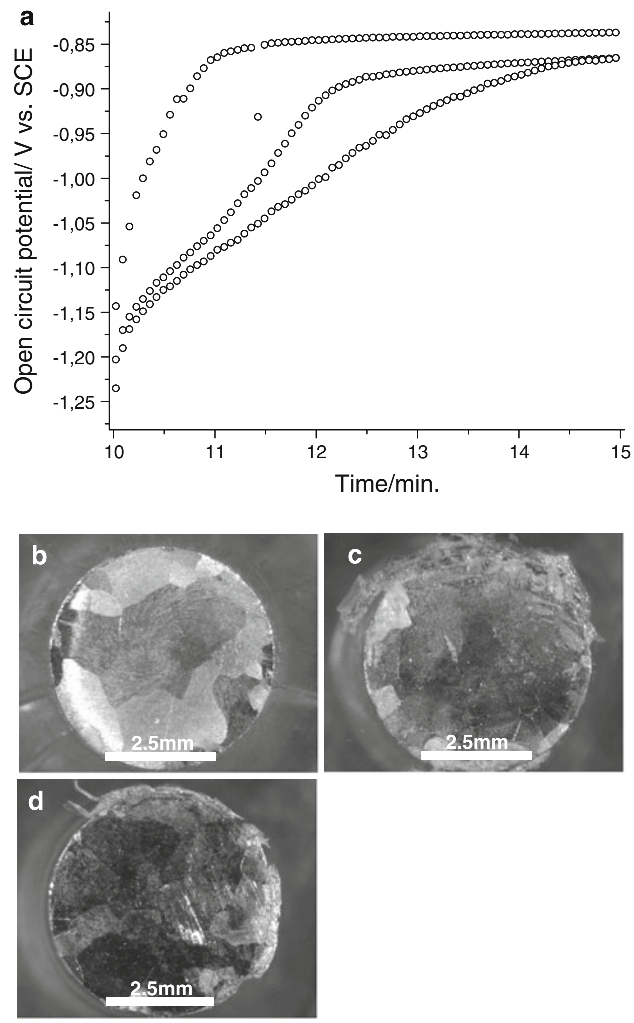

Fig. 5 Results of replicate experiments for large grain size sample at 175 mA cm^{-2} in 0.5 M $KHCO_3$ for 10 min. **a** open circuit potential transient right after the galvanostatic polarization (**b–d**) surfaces of samples with a weight loss rate of **b** 121.8, **c** −29.1, and **d** 23.4 mg cm^{-2}h^{-1}

rotation rate, similar to what was observed for a decrease in electrolyte concentration (Fig. 7). In addition, the morphology was substantially modified, and the main degradation was the D type. The potential measured as a function of time showed the characteristics mentioned before, such as an increase in the steady-state potential with increasing rotation rate, transition times, and an anodic trend when the steady state was reached.

3.2 Characterization of the degradation morphology

EDS was used to estimate the elemental composition of the deposits. Because most deposits were thinner than the EDS interaction volume, this technique cannot provide an accurate composition of the deposits.

An image of the G type deposit is shown in Fig. 2a. In the corroded grain, Sn (78 wt%), K (4.5 wt%), and O (17 wt%) were detected, while the unattacked grain exhibited only Sn (99 wt%) and K (0.93 wt%).

Due to the fact that Sn and K peaks in the EDS spectra overlap, the hypothesis that K is physically present on the surface needs further experimental verification. From a theoretical point of view, a pure Sn EDS spectrum will show an L α/β height ratio of 0.7. However, the actual measured ratio was higher, which could have been caused by an additional element (e.g., K). In addition, it was observed that if the electrolyte was replaced with a Na-based electrolyte, which has no possible overlap with the Sn peak set, the ratio was exactly 0.7 and a Na peak appeared at lower energies. From those facts, it can be inferred that both Sn and K were on the surface.

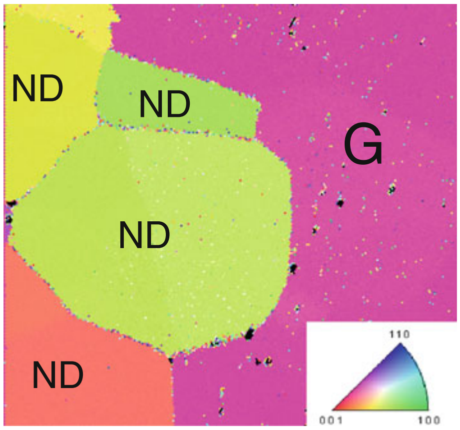

Fig. 6 Map of grain orientations present in a degraded surface after a galvanostatic experiment at 175 mA cm^{-2} in a 0.5 M $KHCO_3$ electrolyte for 5 min. ND indicates that no degradation was present, while G indicates a G type degraded grain

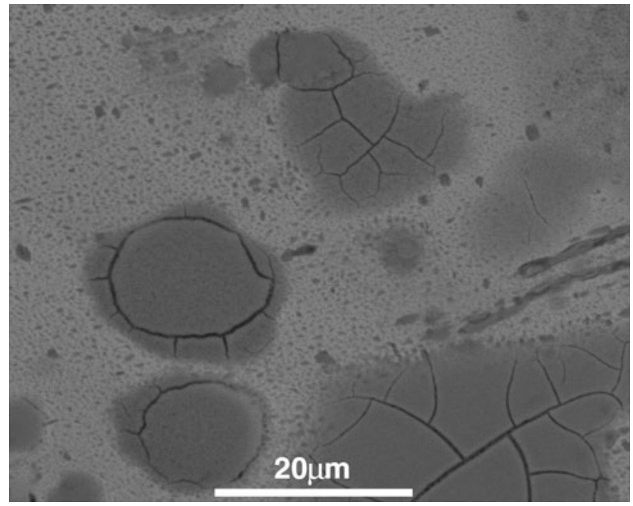

Fig. 8 Back Scattered Electron micrograph of D2 type deposit

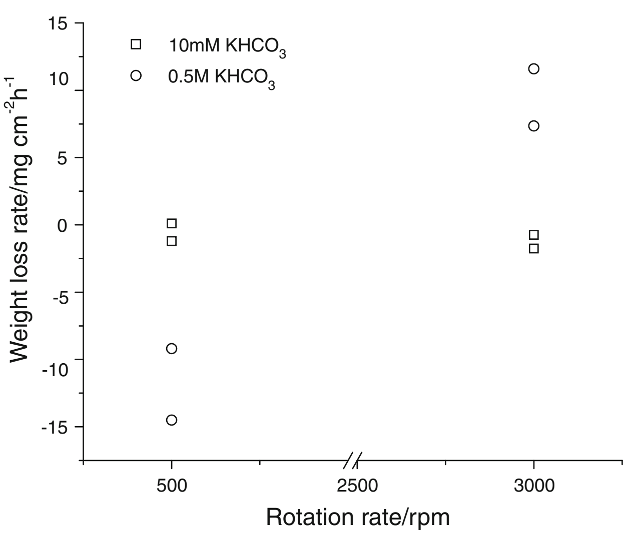

Fig. 7 Weight loss rate as a function of rotation rate for 10 mM and 0.5 M $KHCO_3$ for galvanostatic experiments at 175 mA cm^{-2} with medium grain size for 60 min

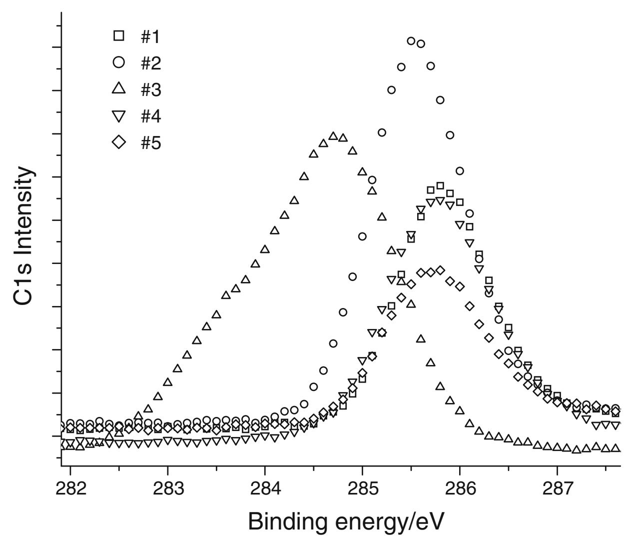

Fig. 9 C1*s* XPS spectra of various samples. For sample #1, the region under analysis was mostly covered with B type, while for samples #2 to #5, a coverage of mostly G and D types were present

Elemental composition of the D2 type (blister-type) deposit was Sn (74 wt%), K (7.34 wt%), O (16 wt%), and C (2.91 wt%). Deposits without C were also measured, indicating that a B type can cover a D type (a stain on top of the blister). The composition of the D1 type was similar to D2. For the case of a Na-based electrolyte, similar compositions were found, except that Na replaced K (No Sn and Na peaks overlapped). The elemental composition of the B type was Sn (89 wt%) and C (11 wt%).

A D2 deposit was analyzed with a Backscattered Electron (BSE) detector, which is sensitive to *z* number of the near-surface region (Fig. 8). A contrast in BSE intensity was observed between the deposits and the Sn surface, with the lower *z*-number elements in the deposit resulting in a darker appearance. Small D type deposits a few microns size suggest a nucleation and growth process.

XPS analysis was performed on various samples to individually characterize the degradation types. However, the inaccuracy of the positioning of the 300 by 700 µm analysis area prevented exact characterization of each degradation type. The samples were selected based on SEM/optical observations. For sample #1, the region under analysis was mostly covered with a B type (G and D also present). For samples #2 to #5, the regions were mostly covered with G and D types. For all the samples, charge neutralization was necessary, indicating that the deposits were less conductive than the original surface. The XPS spectra of all samples detected K with an oxidation state of

+1. In addition, the energy range of the C1*s* peaks (Fig. 9), implied that oxidation states between +2 and +0 were present. Hence, the original C^{4+} in the bicarbonate anion might be reduced to formate or carbon. Other elements, such as Sn and O, were found, confirming what was observed in the EDS spectra.

4 Discussion

Cathodic polarization of Sn in various N_2 saturated solutions resulted in a complex array of degradation morphologies. Under some conditions, weight loss was observed, likely associated with SnH_4(g) formation (or the formation and decomposition of alkali hydrides), whereas under other conditions a weight gain was observed owing to deposits. However, deposits formed even when weight loss was observed, and SnH_4(g) likely formed to a certain extent even when weight gain was observed. Following the results of Salzberg [10, 23], no effort was made in this study to measure the amount of SnH_4(g). H_2 formation would be required for a complete understanding of the reaction kinetics. In addition, all the hypothesized intermediates are highly unstable in aqueous electrolytes, which further complicates quantification of the kinetics.

In an attempt to simplify the situation, the surface morphology was categorized into various types based on the surface characteristics observed in SEM. The primary morphology types were labeled G, D, and B. The G type morphology exhibited a clear image of the surface grain structure because of rate of reaction that varied with grain orientation. The D type morphology was characterized by deposits that were generally more homogeneously distributed over the surface of the electrode. No apparent grain orientation dependence was observed. The B type morphology was associated with regions of the surface rich in carbon. B type deposits could form in the presence of other degradation morphology types such as G or D.

G type attack formed because grains with orientation between [001] and [110] exhibited faster rates of reaction and rougher surfaces. More O was observed by EDS in the more heavily attacked grains compared with those with less attack. G type morphology was observed during the time evolution experiments because favorable orientations were available on the sample surfaces. However, the samples used for the rotation rate experiments had such orientations mainly on the edges. A number of experimental factors also affected the formation of the G type. An increase in rotation rate decreased the extent of G type corrosion in favor of the D type. By decreasing either current density or electrolyte concentration, the extent of the G type was also decreased substantially. The G type seemed to form faster than the D type. The D type was only observed after extended times, whereas G type morphology was observed even at 5 min.

EDS analysis of the D type deposits did not clearly identify their composition. However, in agreement with Kiseleva [13], several observations suggest that the D type was an alkali metal compound such as a hydride. EDS and XPS indicated the presence of alkali metals (K^+ or Na^+) in these deposits. Furthermore, the OCP transient measured right after a galvanostatic experiment exhibited a shoulder at approximately −1.1 V SCE, suggesting decomposition of such an unstable compound, and the subsequent WLR was higher (Fig. 5). Formation of the D type morphology was apparently associated with transport and deposition. A high rotation rate produced a final morphology with a high D coverage, indicating that the formation of the D type was mass transfer controlled. Time evolution experiments showed that the D type deposits were not present in the initial stages of electrolysis ($t < 30$ min) and the potential during the galvanostatic polarization exhibited a transition period that lasted up to 10 min (Fig. 3). Guterman et al. [24] suggested that this transient shape was associated with the electrochemical incorporation of alkalis. They indicated that the process was controlled by several variables such as the rate of diffusion of the alkali to the matrix and the rate of formation of the compound. Higher amounts of the D type morphology for Na^+-based electrolytes might therefore be explained by a higher rate of diffusion of smaller Na^+ cations compared to K^+ cations. In addition, it was found that the extent of the D type was substantially diminished by adding the even larger Cs^+ cation to the solution. The transition time could also be associated with the time required to reach a steady-state coverage of the D type. The duration of the transition time was smaller at higher rotation rates, and the coverage of the D type was higher. This is in agreement with the nucleation and growth process proposed by Guterman et al. [24], in which lower transition times would be followed by a higher coverage of the D type. Experiments at medium current densities increased substantially the yield of the D type deposits while simultaneously the yield of the G type was decreased.

The low coverage of the B type prevented further analysis. However, the B type deposit is found readily in the presence of CO_2, as will be reported in a subsequent publication.

The G type degradation was associated with either weight loss or weight gain. For example, at a high current density and low rotation rate (500 rpm), weight gain was observed. In contrast, in the time evolution experiments, a substantial weight loss was measured (the rate of which decreased as a function of time). Clear evidence of material loss is observed in the G type morphology, so weight was lost even when a net weight gain was observed. A possible

explanation of this behavior is that the high roughness found within attacked grains might contribute to a local decrease in current density (auto-inhibition), which would enhance the formation of the D type within this degraded grain (thus generating a net weight gain). Gradual formation of D type deposits would also explain the decrease of WLR as a function of time (Fig. 4). EDS measurements also supported this hypothesis, showing that the deposits formed on previously generated G type morphologies had compositions similar to D type.

The dispersion observed in all experiments, which has been mentioned by several authors [8–10], can be attributed to the orientation dependence of the G type.

In general, the experiments showed an edge effect, in which the degradation morphology was different in the edge in comparison to the center of the Sn disk. One of the possible causes of this edge effect is the recrystallization of Sn after it was embedded on the acrylic holder. It is known that pure Sn recrystallizes at room temperature and deformation should also induce it on the edges [25]. In addition, the accumulation of bubbles on that region could also cause a large increase in effective current density. Nevertheless, the edge effect usually affected less than 20% of the total electrode area.

5 Conclusions

This study has provided insight into the cathodic degradation morphologies of pure Sn under conditions where CO_2 reduction did not occur. Even though a gaseous Sn hydride is the thermodynamically expected degradation product under cathodic polarization, it is clear that other degradation mechanisms were more relevant. Two main degradation morphologies were identified: G and D.

- The G type was dominated by cathodic corrosion of Sn. The extent of corrosion was strongly dependent on grain orientation and both weight gains and losses were observed for G type attack. It exhibited an auto-inhibiting mechanism, because it generated an increase in surface roughness that reduced its rate of formation. Controlling this type of attack would require careful control of the crystallographic texture.
- The D type was a deposit composed mainly of an alkali coming from the electrolyte (Na^+, K^+, etc.). Small weight change was associated with the D type.

The experimental conditions where these degradation modes occur were clearly established so that further research will fully characterize these different degradation types and further investigate the mechanisms that give rise to these degradation morphologies. The effects of other variables, such as the interaction of bubble coverage with current density and the presence of higher concentration of CO_2 will be analyzed in a subsequent publication.

Acknowledgments The authors would like to thank F. Gambina and M. Kappes for fruitful discussions and N. Kelley for help with the chemical measurements. The project was sponsored by a gift from DNV Research & Innovation, Dublin, Ohio.

References

1. Katsounaros I, Dortsiou M, Kyriacou G (2009) J Hazard Mater 171:323
2. Katsounaros I, Ipsakis D, Polatides C, Kyriacou G (2006) Electrochim Acta 52:1329
3. Katsounaros I, Kyriacou G (2007) Electrochim Acta 52:6412
4. Katsounaros I, Kyriacou G (2008) Electrochim Acta 53:5477
5. Oloman C, Li H (2008) ChemSusChem 1:385
6. Hori Y (2008) In: Vayenas C et al (eds) Modern aspects of electrochemistry, vol 42. Springer, New York, p 89
7. Subramanian K, Asokan K, Jeevarathinam D, Chandrasekaran M (2007) J Appl Electrochem 37:255
8. Gladyshev V (1975) J Appl Chem USSR 48:540
9. Gastwirt LW, Salzberg HW (1957) J Electrochem Soc 104:701
10. Salzberg HW, Mies F (1958) J Electrochem Soc 105:64
11. Salzberg AW, Andreatch AJ (1954) J Electrochem Soc 101:28
12. Winter M, Besenhard JO (1999) Electrochim Acta 45:31
13. Kiseleva IG, Avrutskaya IA, Tomashova NN, Niyazinbetov ME, Fioshin M, Kabanov BN (1976) Sov Electrochem 12:859
14. Cherasev AF, Khrushch AP (1998) Russ J Electrochem 34:410
15. Cherashev AF, Khrushch AP (1997) Russ J Electrochem 33:181
16. Kabanov BN (1968) Electrochim Acta 13:19
17. Courtney IA, Dahn JR (1997) J Electrochem Soc 144:2045
18. Pourbaix M (1974) Atlas of electrochemical equilibria in aqueous solutions. National Association of Corrosion Engineers, Houston
19. Brown CA (1974) J Org Chem 39:3913
20. Mills R, Dayalan E, Ray P, Dhandapani B, He J (2002) Electrochim Acta 47:3909
21. Eigeldinger J, Vogt H (2000) Electrochim Acta 45:4449
22. Dukovic J, Tobias CW (1987) J Electrochem Soc 134:331
23. Salzberg HW, Andreatch AJ (1954) J Electrochem Soc 101:528
24. Guterman V, Averina Yu, Grigor'ev V (1999) Electrochim Acta 45:873
25. Maykuth DJ, Hampshire WB (2003) In: Cramer SD, Covino BS (eds) ASM handbook, vol. 13B: corrosion: materials. ASM, Materials Park, p 177